Perylene derivative charge transfer salts: synthesis, crystal structure and characterisation of $(pet)_3[Ni(mnt)_2]_2$

Jorge Morgado,[a,b] Isabel C. Santos,[a] Luís F. Veiros,[b] Rui T. Henriques,[a,b] M. Teresa Duarte,[b] Manuel Almeida*[a] and Luís Alcácer[b]

[a]*Departamento de Química, Instituto Tecnológico e Nuclear, P-2686 Sacavém Codex, Portugal*

[b]*Departamento de Engenharia Química, Instituto Superior Técnico, P-1096 Lisboa Codex, Portugal*

$(pet)_3[Ni(mnt)_2]_2$ single crystals, where pet = perilo[1,12-*b*,*c*,*d*]thiophene and mnt = maleonitriledithiolate (*cis*-2,3-dimercapto-butene-2,3-dinitrile), were obtained by electrocrystallisation from dichloromethane solutions of pet and the tetrabutylammonium salt of $[Ni(mnt)_2]^-$. The crystal structure is triclinic, space group *P*1, with cell parameters $a = 10.2972(9)$, $b = 11.5037(12)$, $c = 13.3297(10)$ Å, $\alpha = 78.320(8)°$, $\beta = 87.096(7)°$, $\gamma = 87.785(8)°$, $Z = 1$ and consists of segregated stacks along ***a*** of partially oxidised pet molecules arranged as trimers, $(pet)_3^{2+}$, and dimerised $[Ni(mnt)_2]^-$ anions. The electrical properties are typical of a semiconductor with room-temperature conductivity of *ca.* 9 S cm^{-1} with an activation energy of 168 meV, and the paramagnetic susceptibility is due to a singlet–triplet type contribution of antiferromagnetically coupled pairs of $S = 1/2$ spins of the $[Ni(mnt)_2]^-$ species with $J/k_B = -226$ K.

The perylene molecule has been extensively used, for more than 30 years, in the preparation of molecular conductors. Highly conducting or even truly metallic behaviour has been observed in many charge transfer salts of perylene with anions as different as halogens, simple inorganic counter-ions or metallocomplex species.[1] Among the metallocomplexes used as anions, the family of compounds based on metal bisdithiolenes, $M(mnt)_2^-$ (mnt = maleonitriledithiolate), has been extensively studied in our laboratory. While the effects of the counter-ion type variation on the physical properties of these solids have been widely explored, much less is known about the effects of chemical and structural variations on the perylene molecule. Among the few molecular conductors based on perylene modified molecules, there are the charge transfer solids of tetrathioperylene (TTP)[2] and 1,2,7,8-tetrahydrodicyclopenta[*c*,*d*:*l*,*m*]perylene (CPP) with iodine[3] and of CPP with simple inorganic anions.[4,5]

In order to improve the understanding of the effects of perylene chemical modifications in this type of solids, we decided to explore the use of the perilo[1,12-*b*,*c*,*d*]thiophene derivative (pet)[6] as a donor in charge transfer salts. In this paper, we report the synthesis, crystal structure and the electrical and magnetic properties of the charge transfer salt $(pet)_3[Ni(mnt)_2]_2$ for which some preliminary data have been previously reported.[7]

Experimental

Sample preparation

Single crystals of $(pet)_3[Ni(mnt)_2]_2$ were obtained by electrocrystallisation from dichloromethane solutions of pet and $[NBu^n_4][Ni(mnt)_2]$, (5 mmol l^{-1} and 2.5 mmol l^{-1}, respectively) under galvanostatic conditions (*ca.* 2 μA cm^{-2}) on platinum electrodes and at room temperature. The compound pet was synthesised from 3,4,9,10-perylenetetracarboxylic dianhydride (Aldrich) according to the procedure of Rogovik,[6] but using in the last decarboxylation step the technique described by Iwashima and Aoki,[8] and purified by multiple gradient sublimation (10^{-5} Torr, *ca.* 120 °C). $[NBu^n_4][Ni(mnt)_2]$ was prepared following the procedure of Davison and Holm,[9] and twice recrystallised from acetone–diethyl ether. Dichloromethane (Merck p.a.) was freshly distilled over P_2O_5 just before use, and the electrocrystallisation solutions were argon deaerated. Dark crystals as elongated thin plates of $(pet)_3[Ni(mnt)_2]_2$, with typical dimensions $2.5 \times 1 \times 0.2$ mm, were collected in the anode compartment after about ten days, washed with dichloromethane and kept under argon atmosphere in order to prevent a slow decomposition noticed as a surface whitening after a few days at ambient atmosphere.

X-Ray structure determination

A single crystal with approximate dimensions $0.5 \times 0.5 \times 0.2$ mm was glued to a glass capillary mounted in a goniometer head placed on an Enraf-Nonius CAD-4 automatic diffractometer. X-Ray data were collected at room temperature by using graphite-monochromated Mo-Kα ($\lambda = 0.710\,69$ Å, 50 kV, 32 mA) radiation up to 2θ 56° (index ranges $-1 \leqslant h \leqslant 13$, $-15 \leqslant k \leqslant 15$, $-17 \leqslant l \leqslant 17$), in the ω–2θ scan mode [$\Delta\omega = (0.85 + 0.35 \tan\theta)°$]. Unit-cell parameters (Table 1) and the orientation matrix were obtained from least-squares refinement of the setting angles of 25 reflections in the range $24° < 2\theta < 34°$. The intensities were corrected for Lorentz, polarisation and absorption effects by empirical corrections based on ψ-scan (maximum and minimum transmission factors were 0.9997 and 0.9332), using the Enraf-Nonius reduction program. The structure was solved by direct methods, using SHELX-86,[10] and subsequently completed by Fourier recycling, using SHELXL-93.[11] As a non-centrosymmetric structure it was refined as a twin with a Flack parameter of 0.69(2). All

Table 1 Crystal data for $(pet)_3[Ni(mnt)_2]_2$

empirical formula	$C_{76}H_{30}N_8Ni_2S_{11}$
formula mass	1525.16
crystal system	triclinic
space group	*P*1
a/Å	10.2972(9)
b/Å	11.5037(12)
c/Å	13.3297(10)
α/degrees	78.320(8)
β/degrees	87.096(7)
γ/degrees	87.785(8)
V/Å^3	1543.7(2)
Z	1
D_c/Mg m^{-3}	1.641
μ/mm^{-1}	1.039
reflections collected	8648
data/parameters	8648/872

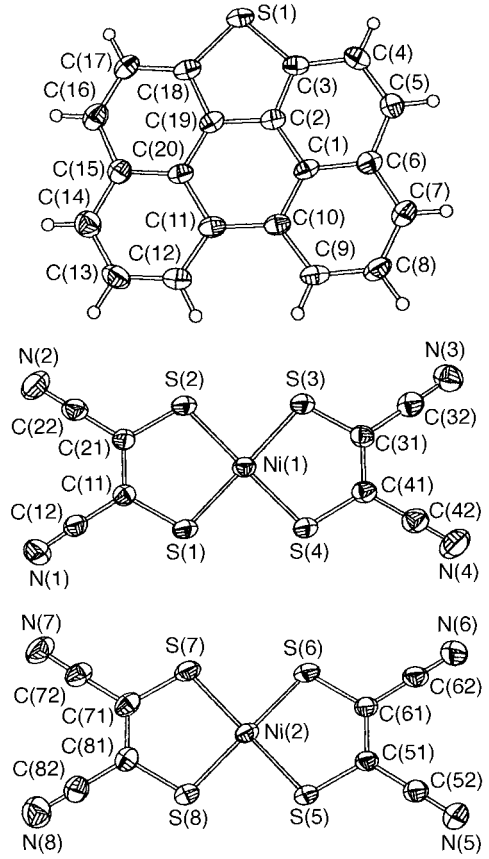

Fig. 1 Thermal ellipsoid drawing (40% probability) and numbering schemes for a pet unit and for the two crystallographically independent $Ni(mnt)_2$ units in $(pet)_3[Ni(mnt)_2]_2$

non-hydrogen atoms were refined anisotropically. The hydrogen atoms were set in calculated positions. Final refinement on F_o^2 by full-matrix least-squares techniques with anisotropic thermal displacement parameters for the non-hydrogen atoms converged at $R=0.0392$, $R_w=0.0847$, $[I>2\sigma(I)]$, $S=0.973$. A difference Fourier synthesis revealed residual densities between -0.418 and 0.412 e $Å^{-3}$. Molecular numbering schemes for a pet unit and for the two crystallographically independent $Ni(mnt)_2$ units of $(pet)_3[Ni(mnt)_2]_2$ are shown in Fig. 1. Selected bond lengths and angles for the two $Ni(mnt)_2$ units are given in Table 2. Atomic coordinates, thermal parameters and bond lengths and angles, have been deposited at the Cambridge Crystallographic Data Center (CCDC). See Information for Authors. *J. Mater. Chem.*, 1997, Issue 1. Any request to the CCDC for this material should quote the full literature citation and the reference number 1145/55.

Electrical transport and magnetic measurements

Electrical resistivity and thermoelectric power measurements were performed in single crystals, placed in a cell, attached to the cold finger of a closed cycle refrigerator, with an accessible temperature range of 18–310 K. Electrical contacts were made by attaching gold wires with platinum paint to gold pads previously evaporated around the crystal. In a first step, the thermopower was measured along the needle axis ***a*** of the sample, using an apparatus similar to that originally described by Chaikin and Kwak,[12] with thermal gradients of 1 K. The crystal was directly attached to two $\phi=25$ μm 99.999% pure gold wires (Goodfellow Metals) with platinum paint and the thermal gradients were monitored with Au(0.07 atom% Fe)–chromel thermocouple. The absolute thermopower was calculated after the correction for the absolute thermopower of gold, using the data of Huebner.[13]

Electrical resistivity was measured without removing the sample from the thermopower cell by attaching to it two additional gold wires, in order to obtain a four-in-line electrode configuration. Measurements were performed with a 1 μA low frequency (77 Hz) current, the voltage being measured with a lock-in amplifier (EG&G PAR 5301). The samples were previously checked for unnested/nested voltage ratios[14] that were kept below 5%.

Static magnetic susceptibility was measured in the range 4–300 K by the longitudinal Faraday system, using an Oxford Instruments system with a field of 3.5 T and a gradient of 5 T m^{-1}.

Results and Discussion

The $(pet)_3[Ni(mnt)_2]_2$ crystal structure, which is non-centrosymmetric, consists of segregated stacks of pet units arranged as trimers and $Ni(mnt)_2$ units arranged as dimers, both along the ***a*** axis (see Fig. 2 and 3). While the organic pet units are essentially planar and, within 1°, parallel to each other (their normals make angles of between 12 and 13° with the ***a*** axis), the inorganic anions $Ni(mnt)_2$ present a strong curvature and are more tilted (the normal to their average plane makes an angle of 47° with the stacking axis ***a***) (see Fig. 3).

The distances between average pet planes are: petA—petB = 3.37 Å, petA—petC = 3.23 Å and petC*—petB = 3.47 Å, as identified in Fig. 3, and their overlap modes are shown in Fig. 4. The overlap mode with longer distance between petC* and petB molecules, with the S atoms in the same side [Fig. 4(a)], is obtained by a slip of the molecules along their long axis and it is essentially a graphite like mode, as observed in several highly conducting perylene based conductors,[1] such as the α-$(perylene)_2M(mnt)_2$ compounds with M = Pt, Au, Ni, Cu, Fe and Co, where the interplanar distances are shorter (in the range 3.32–3.36 Å),[15–18] or $CPP_2(I_3)_{1-\delta}$ where the interplanar distance is 3.41 Å.[3] The two other overlap modes, between molecules with S atoms pointing in opposite sides [Fig. 4(b) and (c)], are obtained essentially by a slip of the molecules along the axis containing the S atom, in a fashion similar to that found in the perylene trimer of $(perylene)_4[Co(mnt)_2]_3$.[19] Within experimental error, the pet units are planar. The comparison of their geometry with that of neutral pet, whose structure was recently obtained by us,[20] reveals small but significant differences (see Table 3), suggesting an uneven charge distribution, more localised in molecules A and B.

The $Ni(mnt)_2$ stacks are dimerised, with the two overlap modes shown in Fig. 4(d) and 4(e). Mode I, Fig. 4(d), between units at a larger average interplanar distance of 3.64 Å, denotes a distorted metal over sulfur arrangement leading to a distorted pyramidal coordination of the Ni atom with an apical Ni—S bond length of 3.85 (5) Å and a Ni—Ni distance of 4.31 (4) Å. While the Ni atom lies in the plane of the four basal sulfur atoms, the Ni—S apical bond is significantly distorted, making an angle of 71.98° with the basal plane. Mode II, Fig. 4(e), between units at an average interplanar distance of 3.41 Å presents much larger Ni—Ni distances at 6.31 Å. This type of dimer arrangement of the $Ni(mnt)_2$ units in dimers, with the nickel atoms coordinated by five sulfur atoms was previously described in $[PPh_3Me][Ni(mnt)_2]$,[21] $[NEt_4][Ni(mnt)_2]$[22] and $[NPhMe_3][Ni(mnt)_2]$,[23] and it is well known in other similar $Fe(mnt)_2$ and $Co(mnt)_2$ based compounds. However, the apical Ni—S distances in these three compounds (3.59, 3.686 and 3.53 Å, respectively) are shorter.

As indicated by dotted lines in Fig. 2, there are sizeable interactions between the sulfur atoms of the pet units B and C and the $Ni(mnt)_2$ units, as denoted by the S(1)—S(B) and S(6)—S(C) distances of 3.545 and 3.512 Å, respectively, much shorter than the sum of the van der Waals radii (3.70 Å), Table 4.

The outer CN groups of the mnt ligands are significantly

Table 2 Bond lengths (Å) and angles (degrees) for the crystallographically independent $Ni(mnt)_2$ units of $(pet)_3[Ni(mnt)_2]_2$

Ni(1)—S(1)	2.137(2)	Ni(1)—S(3)	2.138(2)	Ni(1)—S(2)	2.143(2)
Ni(1)—S(4)	2.149(2)	S(1)—C(11)	1.727(5)	C(11)—C(21)	1.383(6)
C(11)—C(12)	1.426(8)	C(12)—N(1)	1.129(7)	S(2)—C(21)	1.710(5)
C(21)—C(22)	1.415(7)	C(22)—N(2)	1.141(7)	S(3)—C(31)	1.697(6)
C(31)—C(41)	1.389(6)	C(31)—C(32)	1.427(8)	C(32)—N(3)	1.145(7)
S(4)—C(41)	1.711(6)	C(41)—C(42)	1.450(8)	C(42)—N(4)	1.124(7)
S(1)—Ni(1)—S(3)	178.94(7)	S(1)—Ni(1)—S(2)	92.20(6)		
S(3)—Ni(1)—S(2)	86.96(6)	S(1)—Ni(1)—S(4)	88.40(6)		
S(3)—Ni(1)—S(4)	92.41(6)	S(2)—Ni(1)—S(4)	177.29(8)		
C(11)—S(1)—Ni(1)	103.7(2)	C(21)—C(11)—C(12)	121.6(5)		
C(21)—C(11)—S(1)	120.4(4)	C(12)—C(11)—S(1)	118.0(4)		
N(1)—C(12)—C(11)	177.0(6)	C(21)—S(2)—Ni(1)	104.8(2)		
C(11)—C(21)—C(22)	122.2(5)	C(11)—C(21)—S(2)	119.0(4)		
C(22)—C(21)—S(2)	118.9(4)	N(2)—C(22)—C(21)	179.3(6)		
C(31)—S(3)—Ni(1)	104.0(2)	C(41)—C(31)—C(32)	121.9(5)		
C(41)—C(31)—S(3)	120.4(4)	C(32)—C(31)—S(3)	117.8(4)		
N(3)—C(32)—C(31)	178.4(6)	C(41)—S(4)—Ni(1)	103.5(2)		
C(31)—C(41)—C(42)	121.6(5)	C(31)—C(41)—S(4)	119.7(4)		
C(42)—C(41)—S(4)	118.7(4)	N(4)—C(42)—C(41)	179.3(6)		
Ni(2)—S(6)	2.139(2)	Ni(2)—S(5)	2.143(2)	Ni(2)—S(7)	2.144(2)
Ni(2)—S(8)	2.145(2)	S(5)—C(51)	1.723(5)	C(51)—C(61)	1.374(6)
C(51)—C(52)	1.415(7)	C(52)—N(5)	1.156(7)	S(6)—C(61)	1.712(5)
C(61)—C(62)	1.443(8)	C(62)—N(6)	1.134(7)	S(7)—C(71)	1.722(6)
C(71)—C(81)	1.372(7)	C(71)—C(72)	1.426(7)	C(72)—N(7)	1.138(7)
S(8)—C(81)	1.715(6)	C(81)—C(82)	1.440(8)	C(82)—N(8)	1.118(8)
S(6)—Ni(2)—S(5)	91.96(6)	S(6)—Ni(2)—S(7)	88.35(6)		
S(5)—Ni(2)—S(7)	177.81(8)	S(6)—Ni(2)—S(8)	178.85(7)		
S(5)—Ni(2)—S(8)	87.34(6)	S(7)—Ni(2)—S(8)	92.32(7)		
C(51)—S(5)—Ni(2)	104.4(2)	C(61)—C(51)—C(52)	122.2(5)		
C(61)—C(51)—S(5)	118.9(4)	C(52)—C(51)—S(5)	118.8(4)		
N(5)—C(52)—C(51)	179.4(6)	C(61)—S(6)—Ni(2)	104.1(2)		
C(51)—C(61)—C(62)	121.1(5)	C(51)—C(61)—S(6)	120.6(4)		
C(62)—C(61)—S(6)	118.3(4)	N(6)—C(62)—C(61)	179.1(6)		
C(71)—S(7)—Ni(2)	103.5(2)	C(81)—C(71)—C(72)	121.2(5)		
C(81)—C(71)—S(7)	120.2(4)	C(72)—C(71)—S(7)	118.6(4)		
N(7)—C(72)—C(71)	179.1(6)	C(81)—S(8)—Ni(2)	103.9(2)		
C(71)—C(81)—C(82)	121.6(5)	C(71)—C(81)—S(8)	119.9(5)		
C(82)—C(81)—S(8)	118.5(4)	N(8)—C(82)—C(81)	178.7(6)		

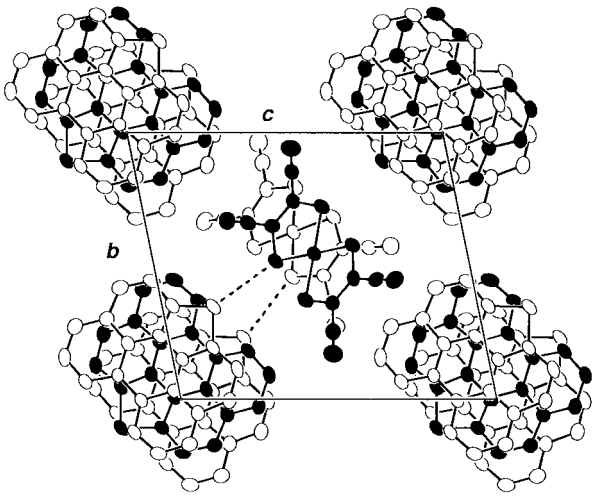

Fig. 2 Projection of the $(pet)_3[Ni(mnt)_2]_2$ crystal structure along the ***a*** axis. The dotted lines indicate short S—S distances between pet and $Ni(mnt)_2$ units. The hydrogen atoms are omitted for clarity.

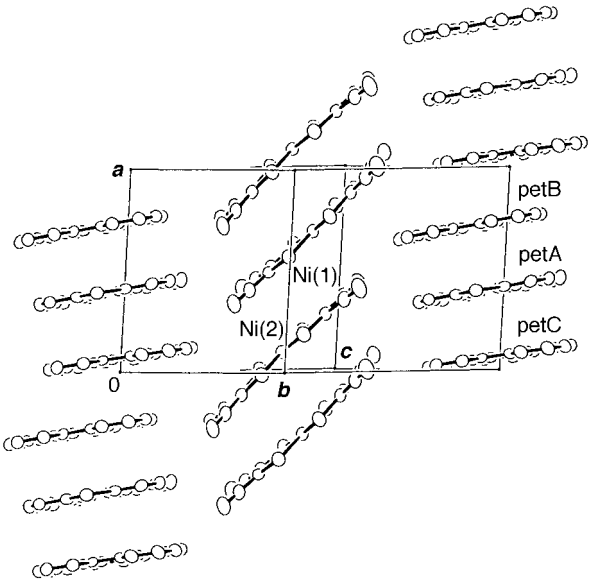

Fig. 3 Side view of the $[Ni(mnt)_2]_2$ stacks locked between the pet stacks

bent out of the NiS_4 plane and towards the closest $Ni(mnt)_2$ unit. This distortion can be understood as a consequence of the tight locking of the $Ni(mnt)_2$ units between the pet stacks as shown in Fig. 3. This is also denoted by several other distances, shorter than the sum of the van der Waals radii, between hydrogen atoms in the different pet units and nitrogen atoms of the ligands, as indicated in Table 4. Rather than hydrogen bonds, the short contacts between the N and H atoms are due to the tight fitting of the molecules in the structure, contributing to the steric displacement of the CN groups out of the NiS_4 plane.

The electrical transport measurements along the stacking axis ***a*** revealed a semiconducting behaviour in the range 100–310 K. The electrical resistivity, ρ, in the range 210–310 K follows a fairly linear dependence of log ρ *vs.* $1/T$ with an

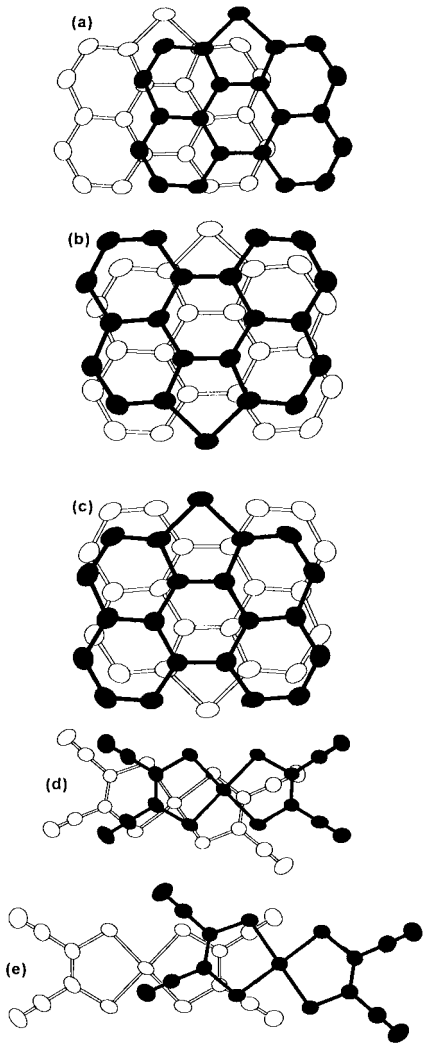

Fig. 4 Molecular overlap modes in $(pet)_3[Ni(mnt)_2]_2$. (a), (b) and (c) between pet units; (d), (e) between $Ni(mnt)_2$ units.

activation energy of 0.168 eV. Upon cooling, a decrease in the activation energy occurs around 200 K, which in the range 100–150 K becomes $\approx$0.08 eV. The semiconducting behaviour in this compound is confirmed by thermopower, which is positive at room temperature and becomes increasingly negative upon cooling. At 200 K a change of regime is also noticed, most probably due to a change from intrinsic to extrinsic behaviour (Fig. 5).

Aiming at testing the electronic dimensionality and calculating the band structure of this solid, the electronic structure of the pet molecule was studied, in a first step, by means of molecular orbital calculations, based on the extended Hückel method[24] with modified H_{ij} values.[25] The HOMO of pet thus obtained is a π orbital, based on a combination of carbon $p_\perp$ orbitals, in which the main contributors are the same as those in the perylene molecule HOMO.[26] The two orbitals present also identical energy and energy separation from the closest orbitals (SOMO and LUMO). A very similar situation was also found in CPP.[3]

The electronic dimensionality of the solid was first tested by means of the evaluation of all the interactions between pairs of next neighbour molecules, through the calculation of the interaction energies, $\beta_{ij} = <\varphi_i|H_{\text{eff}}|\varphi_j>$,[27] between the relevant frontier orbitals of each pair of neighbour molecules, φ_i and φ_j being the HOMO of the pet molecule and both the HOMO and the LUMO of the $[Ni(mnt)_2]$ complex.

Nineteen different contacts were found between pairs of neighbour molecules. Three are along the pet stacks, two along the Ni-complex stacks and the remaining fourteen correspond to side interactions between pet and Ni-complex units. The calculated interaction energies, β, for these contacts are significantly higher when the interactions are along the stacks (see Table 5), showing a clear one-dimensional character of the solid electronic structure. In fact, from all the side interactions, the largest one has a value of $\beta = 54.3$ meV, and the remaining thirteen have interaction energies below 6 meV.

The interaction energy values presented in Table 5 are similar

Table 3 Bond lengths (Å) of neutral pet and pet units in $(pet)_3[Ni(mnt)_2]_2$; + and − signs denote important variations from the neutral species

	petA		petB		petC		neutral pet
S(1)−C(18)	1.750(5)		1.756(5)		1.753(5)		1.753(2)
S(1)−C(3)	1.758(5)		1.756(5)		1.760(4)		1.759(2)
C(1)−C(2)	1.399(6)		1.381(6)	−	1.388(6)		1.399(3)
C(1)−C(10)	1.419(6)		1.416(7)		1.429(6)		1.418(3)
C(1)−C(6)	1.426(7)		1.416(6)		1.425(7)		1.425(3)
C(2)−C(3)	1.381(6)		1.398(7)	+	1.400(6)	+	1.377(3)
C(2)−C(19)	1.402(6)		1.408(6)		1.402(7)		1.408(3)
C(3)−C(4)	1.415(7)		1.391(7)	−	1.400(7)		1.417(3)
C(4)−C(5)	1.379(7)		1.372(7)		1.375(7)		1.368(3)
C(5)−C(6)	1.420(6)		1.438(7)		1.428(6)		1.432(3)
C(6)−C(7)	1.392(6)	−	1.394(7)		1.398(6)		1.411(3)
C(7)−C(8)	1.394(7)	+	1.378(7)		1.372(6)		1.367(3)
C(8)−C(9)	1.384(7)		1.394(7)		1.392(7)		1.402(3)
C(9)−C(10)	1.409(6)	+	1.400(6)		1.398(6)		1.386(3)
C(10)−C(11)	1.467(7)		1.477(6)		1.482(6)		1.481(3)
C(11)−C(12)	1.400(6)		1.396(6)		1.383(6)		1.383(3)
C(11)−C(20)	1.433(6)		1.432(6)		1.425(6)		1.432(3)
C(12)−C(13)	1.384(7)		1.399(7)		1.398(7)		1.398(3)
C(13)−C(14)	1.383(7)		1.379(7)		1.372(7)		1.374(3)
C(14)−C(15)	1.398(7)		1.384(6)		1.414(7)		1.401(3)
C(15)−C(20)	1.407(7)		1.417(7)		1.418(7)		1.411(3)
C(15)−C(16)	1.436(6)		1.430(6)		1.437(6)		1.436(3)
C(16)−C(17)	1.371(7)		1.364(7)		1.377(7)		1.369(3)
C(17)−C(18)	1.422(7)		1.413(7)		1.402(7)		1.410(3)
C(18)−C(19)	1.390(6)		1.390(6)		1.391(6)		1.382(3)
C(19)−C(20)	1.393(6)		1.380(6)		1.393(6)		1.397(3)

Table 4 Short contact distances between pet and $Ni(mnt)_2$ units

atoms	distance/Å	*symmetry operation
S(1)−S(1B*)	3.545	*x*, *y*, *z*
S(1)−C(61*)	3.494	*x*, *y*, *z*
S(6)−S(1C*)	3.512	*x*, *y*, *z*
N(1)−H(13A*)	2.574	0, 1, −1
N(5)−H(4A*)	2.564	*x*, *y*, *z*
N(7)−H(4B*)	2.618	−1, 0, 0
N(7)−H(14B*)	2.627	−1, −1, 0

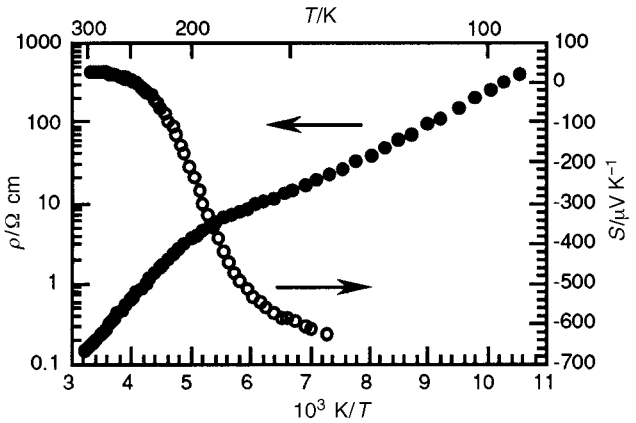

Fig. 5 Electrical resistivity, ρ, and absolute thermoelectric power, S, measured along the ***a*** axis of $(pet)_3[Ni(mnt)_2]_2$, as a function of temperature T

Table 5 Interaction energies, β, for the pet–pet and $[Ni(mnt)_2]$–$[Ni(mnt)_2]$ contacts along the stacks

contact	β_{ij}/meV
pet–pet	
A–B (inside unit cell)	380.8
A–C (inside unit cell)	302.1
B–C* (between unit cells)	335.7
$[Ni(mnt)_2]$–$[Ni(mnt)_2]$	
1–2 (inside unit cell)	116.7
1–2* (between unit cells)	217.2

to the ones found for this type of solids.[3,26,28] However, it should be noted that the value of β for the interaction between pet molecules A–C, inside the unit cell and at shorter distance, is smaller than the one corresponding to the contacts between pet molecules B–C* in neighbouring unit cells and at higher distance. This is due to the different overlap modes between these molecules (Fig. 4). The overlap mode observed between molecules A–B and A–C, corresponding to a slip of the molecules along their short axis, is the same as the one found for $(perylene)_3[FeCl_4]$,[28] where the obtained β values are slightly smaller, owing to longer molecule separation distances. The overlap mode between molecules B–C*, with a slip along the longer dimension of the pet molecule, is the same as the one observed for the $(perylene)_2[M(mnt)_2]$ α-phases,[26] and the obtained β values are similar. In fact, the last type of overlap produces better contacts between the carbon atoms of the adjacent molecules with the highest coefficients on the HOMO of the molecule, resulting in a more efficient interaction.

The interaction energies between $[Ni(mnt)_2]$ complexes are also related with the overlap mode. On one hand, the overlap found inside the unit cell [Fig. 4(e)], corresponding to a shorter interplanar distance (3.41 Å), is obtained by a large slip of the $Ni(mnt)_2$ units along the long axis and produces an interaction with a β value similar to the ones found for the α-phases of the $(perylene)_2[M(mnt)_2]$ compounds.[26] On the other hand, the $[Ni(mnt)_2]$–$[Ni(mnt)_2]$ overlap between adjacent unit cells, although corresponding to a larger interplanar distance (3.64 Å), results in a distorted metal over sulfur geometry, such as the one observed in other dimerised solids, or in the trimerised[19] and polymerised[26] $[Co(mnt)_2]$. This results in a more effective overlap between the metal-complex units, producing a β that is approximately twice the one found for the contact inside the unit cell, and showing the dimerised nature of the $[Ni(mnt)_2]$ stacks in this solid.

It should be also noted that some close distances between sulfur atoms of neighbour pet and complex molecules were found, with values shorter than the sum of the corresponding van der Waals radii (see Table 4). However, these close distances do not present significant values of β, and thus, do not take part in the interactions responsible for the electrical transport in the solid. In fact, as these interactions are the ones between the frontier orbitals of the molecules (the pet HOMO, and the Ni-complex HOMO and LUMO), and since the sulfur atom of the pet molecules presents a practically zero coefficient on the HOMO, the resulting interaction will not involve this orbital and thus will not be reflected on the transport properties. As an example, the β value for the first interaction shown in Table 4 [S(1)—S(1B*)] is $\beta_{LUMO-HOMO}$ = 0.3 meV.

In a second step, and according to the one-dimensional character of the electronic structure, band structure calculations were performed separately for the pet stacks and the Ni-complex ones, using the tight-binding approach[29] of the extended Hückel method.

The results for the pet stacks show a HOMO band split into three portions separated by two gaps, corresponding to the trimerised nature of the stacks. The total width of the band is 0.57 eV, a value that fits well in the range obtained for this type of solid (0.4–0.6 eV).[3,26,28] Assuming an average oxidation degree corresponding to $(pet)_3^{2+}$, the Fermi level lies in the middle of the upper gap, and therefore semiconducting properties, as experimentally observed, are expected. The calculated gap (0.06 eV) in this approach is, however, significantly smaller than the gap obtained from conductivity measurements, a fact that can be attributed to correlation effects, not taken into account by the extended Hückel method.

The calculated band structure of the Ni-complex stacks shows the HOMO and the LUMO bands, each of them divided in two, according to the dimerised nature of the stacks, with a large gap (0.72 eV) separating them. For the assumed average oxidation degree, $[Ni(mnt)_2]_2^{2-}$, the Fermi level of this chain lies in the middle of the LUMO band gap (0.10 eV). The total width of the LUMO band, 0.34 eV, correlates well with that obtained for the LUMO band of the metal-complex stacks, in the α-phases of $(perylene)_2M(mnt)_2$ (0.38 eV).[26]

The full charge transfer, implying the presence of $[Ni(mnt)_2]^-$ anions, is also denoted in the magnetic properties of this compound. For Ni^{III}, in these type of complexes, a $S = 1/2$ state is expected and the paramagnetic susceptibility for a dimerised structure is expected to follow a model of antiferromagnetically coupled pairs of spins. Under these circumstances, the magnetic susceptibility, χ, of this compound was fitted by a model with three types of contributions, as indicated by eqn. (1).

$$\chi = \chi_{S-T} + \chi_o + C/T \quad (1)$$

where χ_{S-T} is the Bleaney–Bowers[30] expression for dimers of antiferromagnetically coupled $S = 1/2$ spins with exchange constant J, as given by eqn. (2),

$$\chi_{S-T} = [2N_A g^2 \mu_B^2/(k_B T)]/[\exp(-2J/k_B T) + 3] \quad (2)$$

with N_A being Avogadro's number, g the Landé factor, μ_B the Bohr magneton, k_B the Boltzman constant and T the absolute temperature. χ_o denotes the temperature independent contributions and the C/T term a possible Curie tail due to impurities or defects.

The experimental $\chi(T)$ results are well fitted by eqn. (1) with a χ_o of -12.5×10^{-4} emu mol^{-1} and a negligible Curie tail. Fig. 6 shows the temperature dependent contribution for χ together with its fit to eqn. (2). A good agreement was obtained with $J/k_B = -226.1(0.5)$ K and $g = 2.336(5)$. It should be mentioned that the estimation of the diamagnetic contribution from tabulated Pascal's constants gives a value of only -7.5×10^{-4} emu mol^{-1}.

Contributions to the magnetic susceptibility similar to this one, and given by eqn. (2), were also found in $[PMePh_3][Ni(mnt)_2]$,[31] $[NEt_4][Ni(mnt)_2]$[31] and

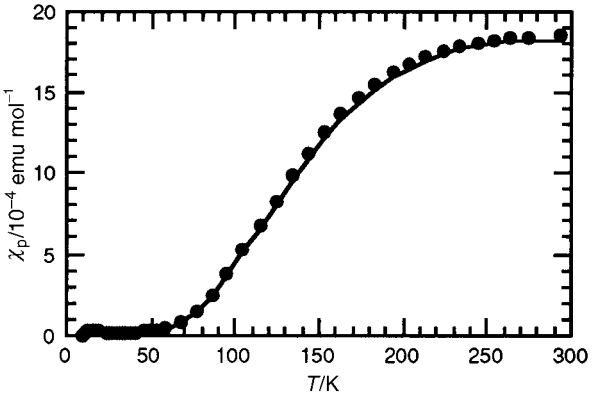

Fig. 6 Paramagnetic susceptibility, χ_P, of $(pet)_3[Ni(mnt)_2]_2$ as a function of temperature. The line is a fit to a singlet–triplet model with $J/k_B = -226$ K.

Table 6 Exchange interaction parameter, J, and geometrical data in different $[Ni(mnt)_2]_2$ based compounds

compound	Ni—S apical distance/Å	$Ni(mnt)_2$ interplanar distance/Å	(J/k_B)/K	ref.
$(pet)_3[Ni(mnt)_2]_2$	3.85	3.64	−226	this work.
$[PPh_3Me][Ni(mnt)_2]$	3.59	3.41	−352.5	21, 31
$[NEt_4][Ni(mnt)_2]$	3.69	3.50	−446	22, 31
$Cs[Ni(mnt)_2]\cdot H_2O$			−197	32

$Cs[Ni(mnt)_2]\cdot H_2O$[32] with J/k_B values of −352.5, −446 and −197 K, respectively. The structure of $Cs[Ni(mnt)_2]\cdot H_2O$, to the best of our knowledge, was not reported. The magnitude and the nature of the magnetic interaction between $Ni(mnt)_2$ anions are expected to vary with the distance and strongly depend on the type of overlap.[31,33] In the other two compounds, basically with the same type of overlap as in $(pet)_3[Ni(mnt)_2]_2$, the larger J values experimentally obtained using eqn. (2) can be ascribed to the shorter distances between the $Ni(mnt)_2$ units (see Table 6). However, it should be also kept in mind that in compounds with stacked structures, as these ones, the J value obtained by fitting experimental data to eqn. (2) is an effective value J_{eff}. This J_{eff} depends not only on the major intradimer interaction J but also reflects the smaller interdimer interaction $J' < J$ that is a function of the separation between the dimers in chains. In this case, an alternating chain model with J and J' would be more appropriate.[34] In such cases J_{eff} estimated by eqn. (2) is smaller than the intrinsic dimer interaction J.[34,35]

This work was partially supported by JNICT under contract PRAXIS/2/2.1/QUI/203/94.

References

1 For a review, see: M. Almeida and R. T. Henriques, in *Handbook of Organic Conductive Molecules and Polymers*, ed. H. S. Nalwa, John Wiley and Sons, Chichester, 1997, vol. 1, ch. 2, p. 87.
2 B. Hilti, C. W. Mayer and G. Rihs, *Solid State Commun*., 1981, **38**, 1129.
3 J. Morgado, I. C. Santos, R. T. Henriques, M. Fourmigué, P. Matias, L. F. Veiros, M. J. Calhorda, M. T. Duarte, L. Alcácer and M. Almeida, *Chem. Mater*., 1994, **6**, 2309.
4 R. Lapouyade, J. P. Morand, D. Chasseau, C. Haw and P. Delhaès, *J. Phys.* (*Paris*) *Coll*., 1983, **44**, C3-1235.
5 P. Penven, D. Jérôme, S. Ravy, P. A. Albouy and P. Batail, *Synth. Met*.,1988, **27**, B405; V. Ilakovac, S. Ravy, A. Moradpour, L. Firlej and P. Bernier, *Phys. Rev. B*, 1995, **52**, 4108; P. Michel, A. Moradpour, P. Penven, L. Firlej, P. Bernier, B. Levy, S. Ravy and A. Zahab, *J. Am. Chem. Soc*., 1990, **112**, 8285.
6 V. I. Rogovik, *J. Org. Chem.* (*USSR*), 1974, **10**, 1072.
7 L. Alcácer, J. Morgado, R. T. Henriques and M. Almeida, *Synth. Met*., 1995, **70**, 1093.
8 S. Iwashima and J. Aoki, *Bull. Chem. Soc. Jpn*., 1968, **41**, 2789.
9 A. Davison and R. H. Holm, *Inorg. Synth*., 1967, **10**, 8.
10 G. M. Sheldrick, SHELXS-86: Program for the Solution of Crystal Structure, University of Göttingen, 1986.
11 G. M. Sheldrick, SHELXL-93: Program for Crystal Structure Refinement, University of Göttingen, 1993.
12 P. M. Chaikin and J. F. Kwak, *Rev. Sci. Instrum*., 1975, **46**, 218.
13 R. P. Huebner, *Phys. Rev*., 1964, **135**, A1281.
14 P. E. Schaffer, F. Wudl, G. A. Thomas, J. P. Ferraris and D. O. Cowan, *Solid State Commun*., 1974, **14**, 347.
15 V. Gama, M. Almeida, R. T. Henriques, I. C. Santos, A. Domingos, S. Ravy and J. P. Pouget, *J. Phys. Chem*., 1991, **95**, 4263.
16 V. Gama, R. T. Henriques, G. Bonfait, L. C. Pereira, J. C. Waerenborgh, I. C. Santos, M. T. Duarte, J. M. P. Cabral and M. Almeida, *Inorg. Chem*., 1992, **31**, 2598.
17 L. Alcácer, H. Novais, F. Pedroso, S. Flandrois, C. Coulon, D. Chasseau and J. Gaultier, *Solid State Commun*., 1980, **35**, 945.
18 A. Domingos, R. T. Henriques, V. Gama, M. Almeida, A. Lopes Vieira and L. Alcácer, *Synth. Met*., 1989, **27**, B411.
19 V. Gama, R. T. Henriques, M. Almeida, L. Veiros, M. J. Calhorda, A. Meetsma and J. L. de Boer, *Inorg. Chem*., 1993, **32**, 3705.
20 I. C. Santos, J. Morgado, T. L. Duarte, L. Alcácer and M. Almeida, *Acta Crystallogr., Sect. C*, in press.
21 C. J. Fritsch Jr., *Acta Crystallogr*., 1966, **20**, 107.
22 A. Kobayashi and Y. Sasaki, *Bull. Chem. Soc. Jpn*., 1977, **50**, 2650.
23 C. Mahadevan, M. Seshasayee, B. V. R. Murthy, P. Kuppusamy and P. T. Manoharan, *Acta Crystallogr., Sect. C*, 1983, **39**, 1335.
24 R. Hoffmann and W. N. Lipscomb, *J. Chem. Phys*., 1962, **36**, 2179; 1962, **37**, 2872; R. Hoffmann, *J. Chem. Phys*., 1963, **39**, 1397.
25 J. H. Ammeter, H. B. Bürgi, J. C. Thibeault and R. Hoffmann, *J. Am. Chem. Soc*., 1978, **100**, 3686.
26 L. F. Veiros, M. J. Calhorda and E. Canadell, *Inorg. Chem*., 1994, **33**, 4290.
27 M. H. Whangbo, J. M. Williams, P. C. W. Leung, M. A. Beno, T. J. Emge and H. H. Wang, *Inorg. Chem*., 1985, **24**, 3500; M. H. Whangbo, J. M. Williams, P. C. W. Leung, M. A. Beno, T. J. Emge, H. H. Wang, K. D. Carlson and G. W. Crabtree, *J. Am. Chem. Soc*., 1985, **107**, 5815.
28 J. A. Ayllón, I. C. Santos, R. T. Henriques, M. Almeida, E. B. Lopes, J. Morgado, L. Alcácer, L. F. Veiros and M. T. Duarte, *J. Chem. Soc., Dalton Trans*., 1995, 3543.
29 M. H. Whangbo, and R. Hoffmann, *J. Am. Chem. Soc*., 1978, **100**, 6093; M. H. Whangbo, W. M. Walsh, jun., R. C. Haddon and F. Wudl, *Solid State Commun*., 1982, **43**, 637; M. H. Whangbo, J. M. Williams, M. A. Beno and J. R. Dorfman, *J. Am. Chem. Soc*., 1983, **105**, 645.
30 B. Bleaney and K. D. Bowers, *Proc. R. Soc. London Ser. A*, 1952, **214**, 351.
31 J. F. Weiher, L. R. Melby and R. E. Benson, *J. Am. Chem. Soc*., 1964, **86**, 4329.
32 A. E. Underhill, P. I. Clemenson, M. B. Hursthouse, R. L. Short, G. J. Ashwell, I. M. Sandy and K. Carneiro, *Synth. Met*., 1987, **19**, 953.
33 A. T. Coomber, D. Beljonne, R. H. Friend, J. L. Brédas, A. Charlton, N. Robertson, A. E. Underhill, M. Kurmoo and P. Day, *Nature* (*London*), 1996, **380**, 144.
34 M. C. Cross and D. S. Fischer, *Phys. Rev. B*, 1979, **19**, 402.
35 J. V. Rodrigues, I. C. Santos, V. Gama, R. T. Henriques, J. C. Waerenborgh, M. T. Duarte and M. Almeida, *J. Chem. Soc., Dalton Trans*., 1994, 2655.

Paper 7/03579I; *Received* 23*rd May*, 1997